Technical Memorandum

SC-TM-69-538
MAY 1970

IMPULSE LOADING OF SINGLE-LAYERED RINGS WITH MAGNETICALLY-DRIVEN FLYER PLATES

H. C. WALLING, 7342
SANDIA LABORATORIES, ALBUQUERQUE

SANDIA LABORATORIES

OPERATED FOR THE UNITED STATES ATOMIC ENERGY COMMISSION BY SANDIA CORPORATION | ALBUQUERQUE, NEW MEXICO, LIVERMORE, CALIFORNIA

SC-TM-69-538

IMPULSE LOADING OF SINGLE-LAYERED RINGS WITH MAGNETICALLY-DRIVEN FLYER PLATES

Harold C. Walling, 7342

May 1970

ABSTRACT

The energy stored in a high-voltage capacitor bank is utilized to propel thin flyer plates. The simplified theory for the flyer plate motion is given. The method of using magnetically-driven flyer plates to impulsively load single-layered isotropic rings over one-half their circumference is described. The experimental-theoretical correlation of the plate motion and the free ring response is discussed.

Issued by Sandia Corporation
a prime contractor to the
United States Atomic Energy Commission

IMPULSE LOADING OF SINGLE-LAYERED RINGS WITH MAGNETICALLY-DRIVEN FLYER PLATES

Introduction

In order to gain confidence in designs based upon sound theory, the systems designer and the theoretician are interested in subjecting the system, or models thereof, to the anticipated environment. Due to various reasons, the laboratory experimenter is obligated to provide various techniques for "simulating" the "actual" environment or effects of the environment. Because of complex and necessary interactions between systems designer, theoretician, and laboratory "simulator," the analyst is interested in evaluating the proposed simulation techniques. The evaluation must begin on simple structural and material models such as isotropic rings and one-dimensional designer's material samples. The purpose of the requested evaluation is to accurately define the experimental technique and to compare the measured response to the theoretical predictions for that particular method. Once this evaluation is made on a particular geometry and set of dimensions, a decision as to the most attractive "simulation" technique for the specific model may be made.

Over the course of the past decade, two general methods for simulating the impulsive surface tractions to structural models have evolved. They are 1) direct explosive loading and 2) high velocity flyer plate loading. Explosive loading methods usually employ thin sheets of explosive such as PETN,

Dupont EL506D detasheet or light-sensitive explosives such as silver acetylide-silver nitrate, as used by SWRI and lead azide under study at Sandia.[1] The explosive may be constructed to provide a particular distribution of impulse by varying its thickness. Detonation is affected by various methods to provide sweeping (axial or circumferential) pressure pulses and quasi-simultaneous loads to the structure's surface. One of the principal objections to the sweeping explosive method is the time associated with propagation of the pressure pulse along the structure's length or circumference depending upon the method of detonation. Detonation is pointwise in the light-sensitive explosive, depending upon the light source spectral intensity and explosive radiation properties. Such pointwise detonation much improves the measure of simultaneous loading imparted to the specimen under study. The flyer plate technique consists of accelerating a thin plate (usually metallic) to high velocity and directing the plate so that it loads the structure in a prescribed manner. The flyer plate may be accelerated by explosives[2] or by electromagnetic forces. The acceleration by capacitor discharge generated electromagnetic forces is for some applications the more controllable and more easily employed driving method. This does not imply that flyer propulsion by electromagnetic forces is superior to acceleration by thin sheet explosive. Through careful alignment of the experimental apparatus, the flyer will provide a very nearly simultaneous, short duration pressure pulse to the structure's surface.

The ability to accelerate thin metal plates to high velocity using high voltage, capacitor discharge systems has been known for some time. It has been only in the last five years that the principle has been applied to structural response experiments. A major part of the development of the technique was performed at EG&G, Inc. in Bedford, Massachusetts through close cooperation with Sandia Laboratories at Livermore.[3] Simultaneously and independently, similar development was underway at the Atomic Weapons Research Establishment, Aldermaston, United Kingdom. Through the efforts of high-voltage capacitor designers such as Maxwell Laboratories in the U.S.A. and the British Insulated Callender's Cables, Ltd. in the United Kingdom, high energy ($> 10^4$ joule), fast discharge (freq.$> 10^5$ Hz) sources for flyer acceleration are readily available. Through the use of these developments the structural response experimenter has enough confidence in the method to compare measurements with theoretical predictions. It is the purpose of this paper to take the first step in the evaluation of this technique for surface loading; that is the method will be defined for a particular experiment. The simplified theory for the response of the flyer plate to the transient magnetic forces is discussed first. A typical ring response experiment is presented in the second section. In the third section the measured ring response is compared with the theoretical predictions.

Theoretical and Experimental Flyer Plate Response

It is well known that two adjacent current carrying conductors experience a repulsive force (if the currents are oppositely directed) due to the magnetic field, B, between them. The force per unit area, P, exerted on two flat, parallel, and closely spaced conductors shown in Fig. 1 is given by:

$$P = \tfrac{1}{2} \frac{B^2}{\mu} \text{ (newton/meter}^2\text{)}, \tag{1}$$

where

$$B = \frac{\mu i}{\delta} \text{ (weber)}, \tag{2}$$

where the magnitude of the current is the same in each conductor, and

δ is the width of the conductor normal to the current direction,

i is the magnitude of current in each plate, and all current elements are assumed strictly parallel and in one-dimension over the total conductor area (the 1D assumption is not valid near the edges of the conductor),

B is the magnitude of the magnetic vector between the conductors,

μ is the relative permeability of the medium separating the conductors (in most cases free space permeability).

Using Eq. (2) in (1) gives

$$P = \tfrac{1}{2} \frac{\mu i^2}{\delta^2} \quad . \tag{3}$$

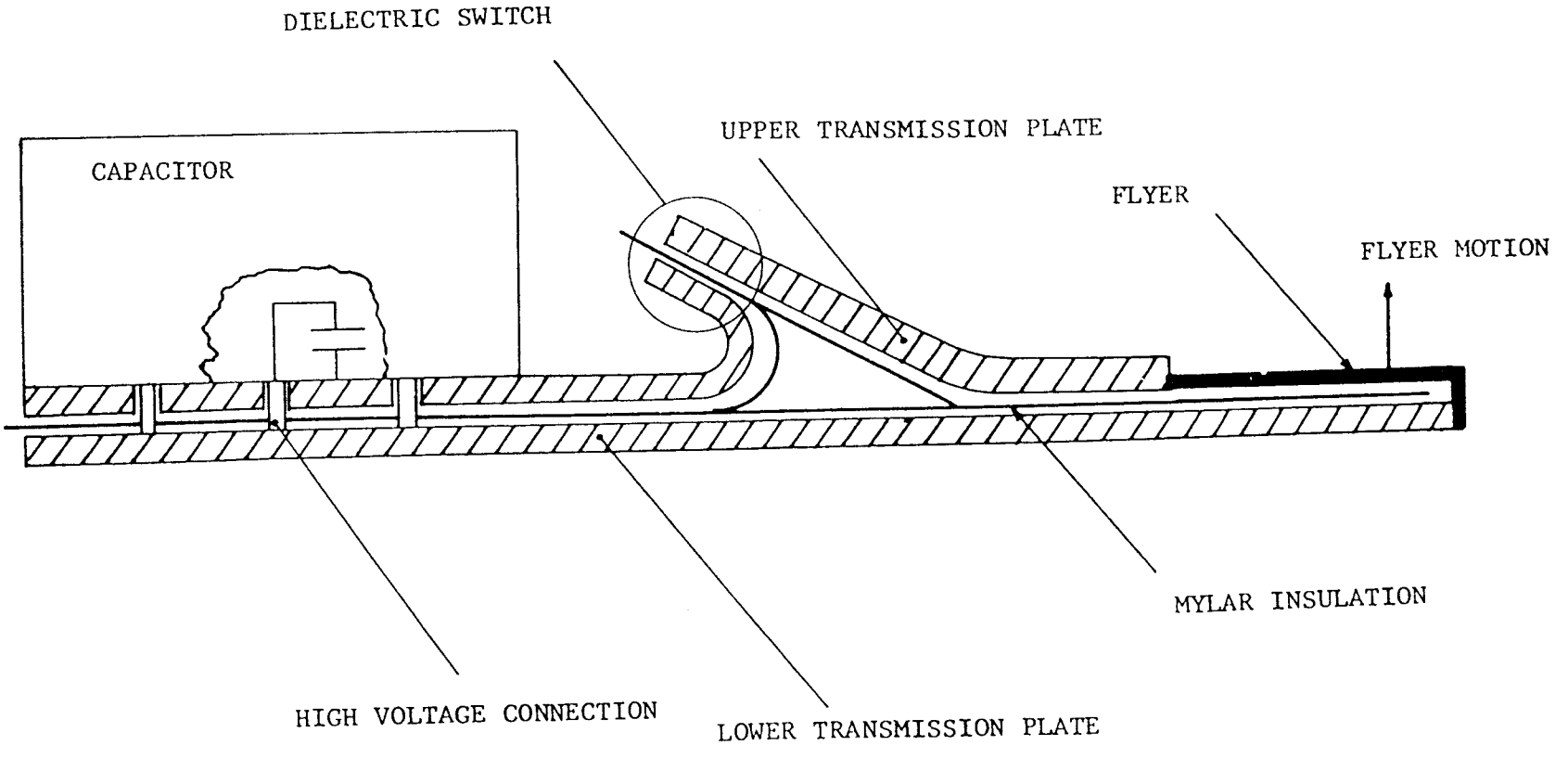

Figure 1. Flat Flyer and Transmission Plate Arrangement.

The acceleration of the plates can be obtained from Eq. (3) by dividing that expression by the mass per unit area of the plate.

$$A(t) = \frac{\mu i^2(t)}{2\rho h \delta^2} \quad \text{(meter/sec)/sec} \quad , \tag{4}$$

where

h is the plate thickness, and

ρ is the plate density.

If the thickness of one plate is made much greater than the other, then the acceleration of the thick plate is much smaller than that of the thin plate and is essentially immovable. In this case the thin plate is called the "flyer" plate and the thick plate is called the "backup" mass. In fast capacitor discharge systems now in use for accelerating flyer plates, large currents ($\sim 10^6$ amperes) are generated. The combination of high currents and thin flyer plates creates large flyer velocities ($\sim$ 1 mm/μs). The capacitor discharge systems used to propel the flyers can be characterized by the circuit shown in Fig. 2. The differential equation for this idealized, lumped parameter circuit is

$$\frac{d(Li)}{dt} + Ri + \frac{1}{C}\int_t i\, dt = V_o \quad , \tag{5}$$

where

$R = R_B + R_L(t)$,

$L = L_B + L_L(t)$,

R_B is the fixed circuit resistance,

$R_L(t)$ is the time dependent circuit resistance,

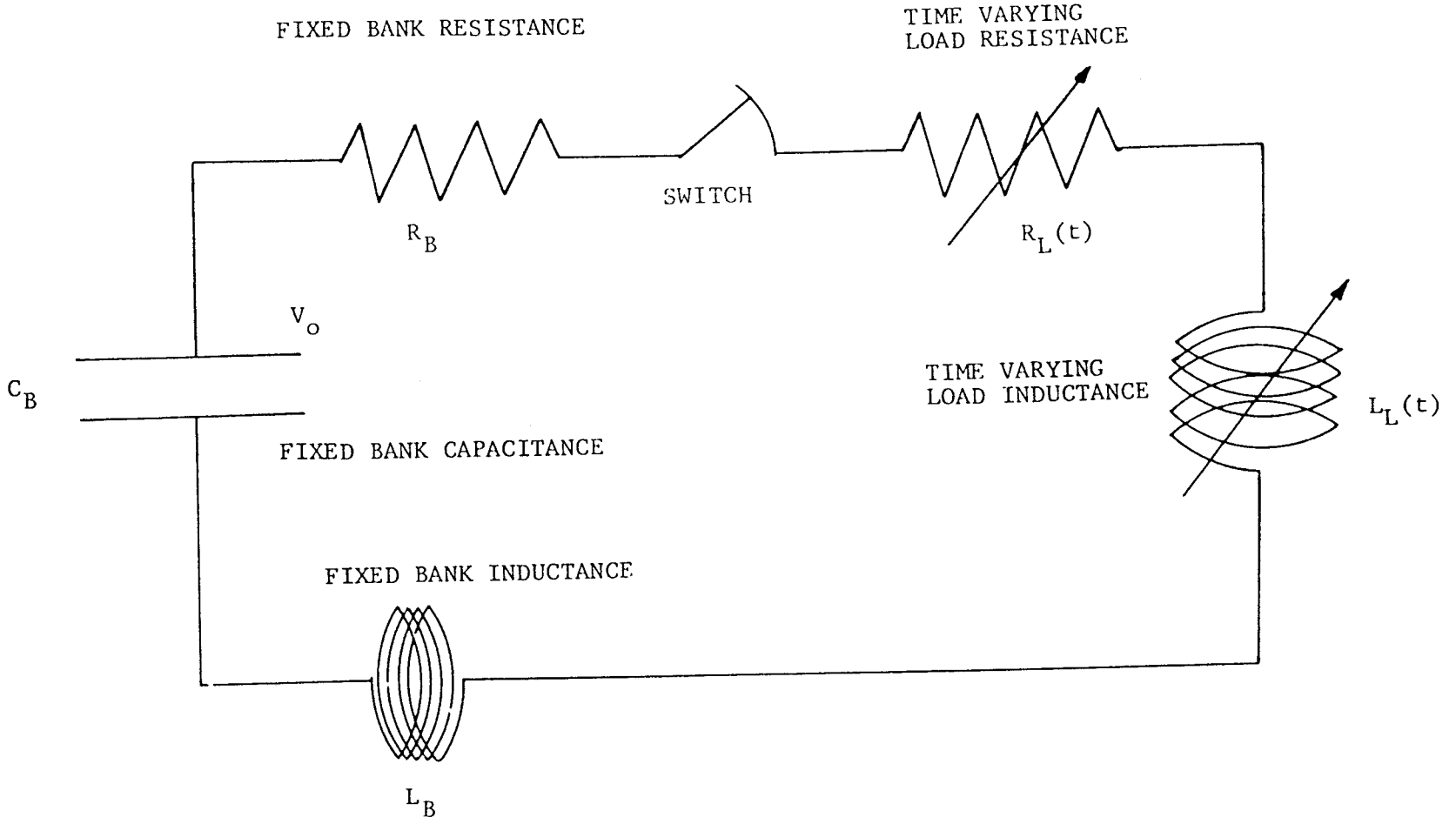

Figure 2. Equivalent Flyer Plate Circuit.

L_B is the fixed system inductance,

$L_L(t)$ is the time dependent load inductance, and

V_o is the initial voltage impressed across the capacitor, C.

If R and L are assumed variable in time, then a time derivative of (5) gives the governing equation for the equivalent lumped parameter circuit current,

$$L\frac{d^2i}{dt^2} + \left(R + 2\frac{dL}{dt}\right)\frac{di}{dt} + \left(\frac{1}{C} + \frac{d^2L}{dt^2} + \frac{dR}{dt}\right) i = 0 \quad . \tag{6}$$

Due to joule heating, the total circuit resistance will increase because most metallic conductors possess electrical resistivities which increase with increasing temperature. The energy dissipated through the circuit resistance is:

$$E_R = \int_o^t i^2 R \, dt \quad .$$

However, one might simplify his calculations if this energy loss is neglected; therefore, R will be assumed time invariant in this first discussion. Refs. 4 and 5 treat the time dependent resistance cases in detail. The displacement S(t) of the flyer plate can be expressed as a double integral on time of Eq. (4) so

$$S(t) = \frac{\mu}{2\rho h \delta^2} \iint_t i^2 \, dt \quad \text{(meter)}. \tag{7}$$

The inductance for two flat, parallel, closely-spaced plates is

$$L_L(t) = \frac{\mu \lambda S(t)}{\delta} \quad \text{(henry)}, \tag{8}$$

where

$$\mu = 4\pi \times 10^{-7} \text{ henry/meter for free space.}$$

When Eq. (7) is substituted into (8) and the derivatives $\frac{dL}{dt}$ and $\frac{d^2L}{dt^2}$ are evaluated from differentiation of Eq. (8) and substituted into Eq. (6), the governing nonlinear, integrodifferential equation is

$$(L_B + \gamma \iint i^2\, dt)\frac{d^2i}{dt^2} + (R + 2\gamma \int i^2\, dt)\frac{di}{dt} + (\gamma i^2 + \frac{1}{C})i = 0, \tag{9}$$

where

$$\gamma = \frac{\mu^2\lambda}{2\delta^3\rho h} \quad .$$

Equation (9) can be solved for i(t) by standard numerical integration techniques on the digital computer.[5,6] The analog computer will also yield solutions for i(t).[7] The velocity at which the flyer moves away from the backup mass can be written as

$$V(t) = \frac{\mu}{2\rho h\delta^2}\int_o^t i^2\, dt \quad . \tag{10}$$

The displacement, S(t), is given in Eq. (8). In the experiment discussed in this paper the parameters of the capacitor discharge system and flyer plate were:

$V_o = 15 \times 10^3$ volts

$C = 27.3 \times 10^{-6}$ farads

$R \approx 12.67 \times 10^{-3}$ ohms

$L_B \approx 26.71 \times 10^{-9}$ henry

$L_L(o) \approx 5.17 \times 10^{-9}$ henry

$h = 3.048 \times 10^{-4}$ meters

$\delta = 3.81 \times 10^{-2}$ meters

$\lambda = .489$ meters

$\rho = 2.71 \times 10^{3}$ kilogram/meter^3

These parameters were used in Eq. (9) to solve for i(t), V(t), and S(t) using fourth order Runge-Kutta and other finite difference numerical integration techniques. Figure 3 shows the predicted current from Eq. (9) compared with the measured current (sensed with a Rogowski probe). The velocity was found for the experiment in question from Eq. (10). Figure 4 is a comparison of the flyer velocity as solved from Eqs. (9) and (10) and digital numerical integration of the measured i^2 vs. t curve.

The displacement-time history of the flyer plate was recorded by a high speed streak camera (Beckman-Wheatley 200). This optically determined displacement as a function of time compared with the solution to Eqs. (8) and (9), and the digital numerical second integration of the measured i^2 vs. t curve is presented in Fig. 5. The discrepancy between the optical determination of S(t) vs. t and the integrated i^2 vs. t curve is due to errors in reducing the streak camera record and the i^2 vs. t record.

Figures 3, 4, and 5 indicate that the lumped parameter, time varying L-R-C circuit is an approximate model for calculating the flyer plate response. The assumptions of no flyer resistance charges [$R \neq R(t)$] and no diffusion of the magnetic field into the flyer plate and backup mass must be reconsidered in order to obtain better agreement between theory and experiment.[8]

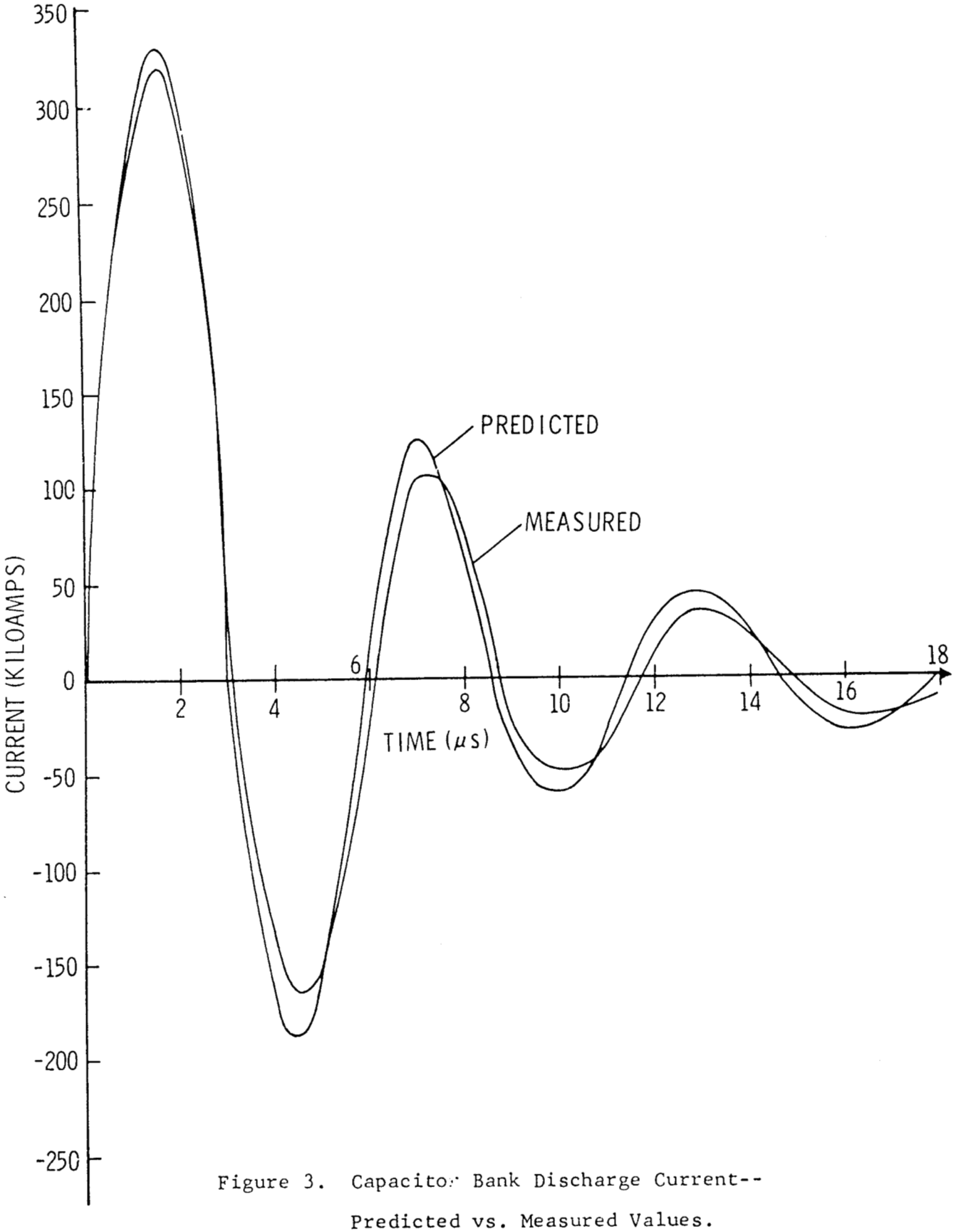

Figure 3. Capacitor Bank Discharge Current--
Predicted vs. Measured Values.

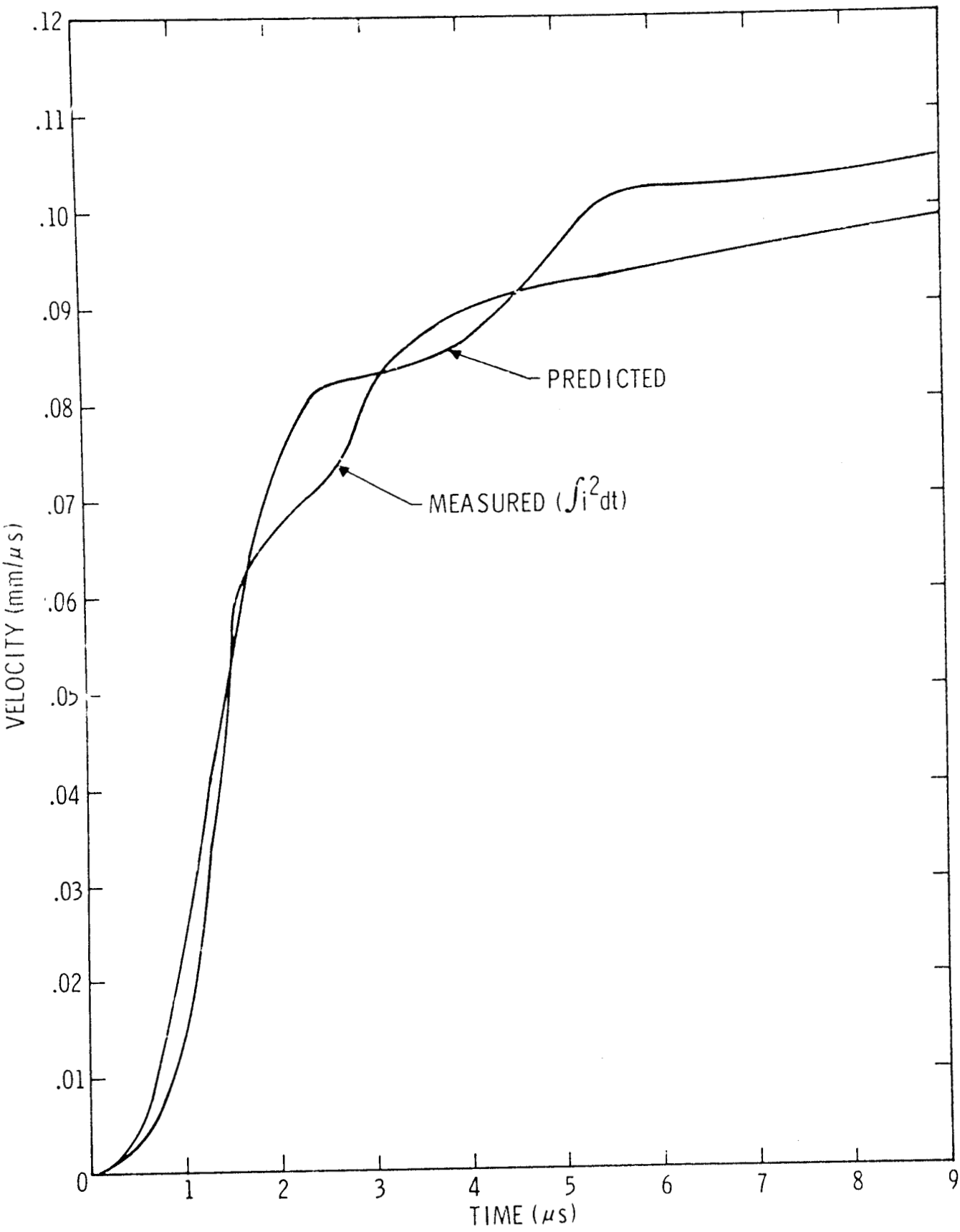

Figure 4. Aluminum Flyer Plate Velocity vs. Time--Predicted vs. Measured Values.

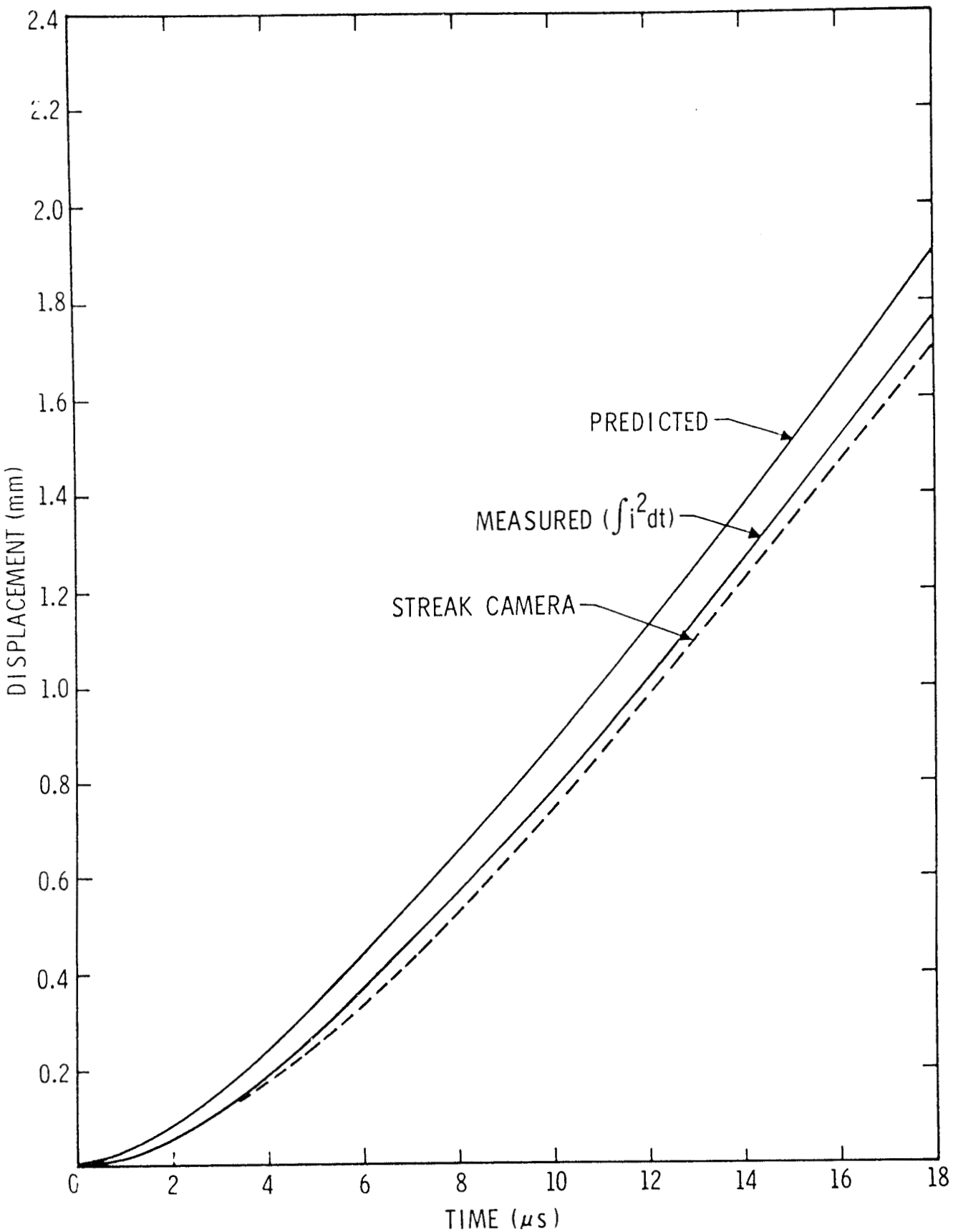

Figure 5. Aluminum Flyer Plate Displacement vs. Time--
Predicted vs. Measured Values.

Description of the Experimental Technique

As shown in the previous section, the flyer motion could be characterized by the solution to the time varying, series L-R-C circuit. These predictions were used as the inputs to the ring response experiment discussed in this section.

Flyer-Ring Geometry

Figure 6 is a schematic of the cylindrical ring-flyer-backup mass arrangement. Figure 7 shows a ring in position to be impacted by the flyer. The ring shown in that photograph is not the actual ring, but it is one used for a particular method of simultaneity assessment. The backup mass was an aluminum piece machined to accommodate the cylindrical flyer and ring with the proper initial flyer-to-ring spacing, $c(\theta,o)$. This spacing must be held to close tolerances in order to provide as nearly a simultaneous arrival as possible. The measurement of simultaneity will be discussed in a later paragraph.

Two θ distributions of specific impulse were selected for study, constant over 170° and cosine over 170°. The flyer was given the desired momentum distribution by altering the width, δ, normal to the direction of current flux in the flyer so that it moved away from the backup mass with a particular velocity distribution in θ. An approximate cosine distribution of velocity can be produced by shaping the flyer as

$$\delta = \frac{\delta_o}{\sqrt{\cos\theta}}$$

where δ is the flyer width at θ and δ_o is the minimum flyer width.

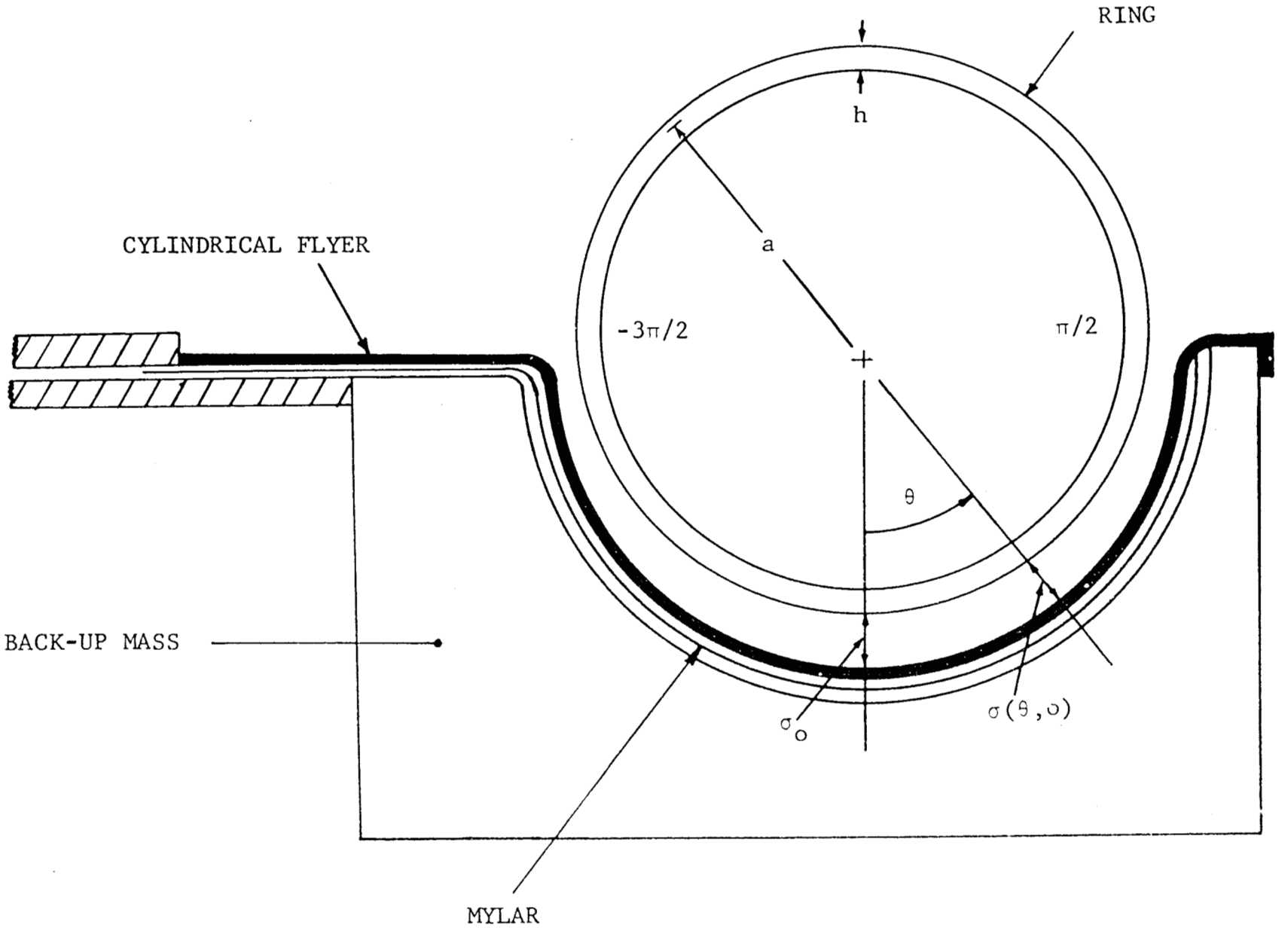

Figure 6. Cylindrical Ring and Flyer Arrangement.

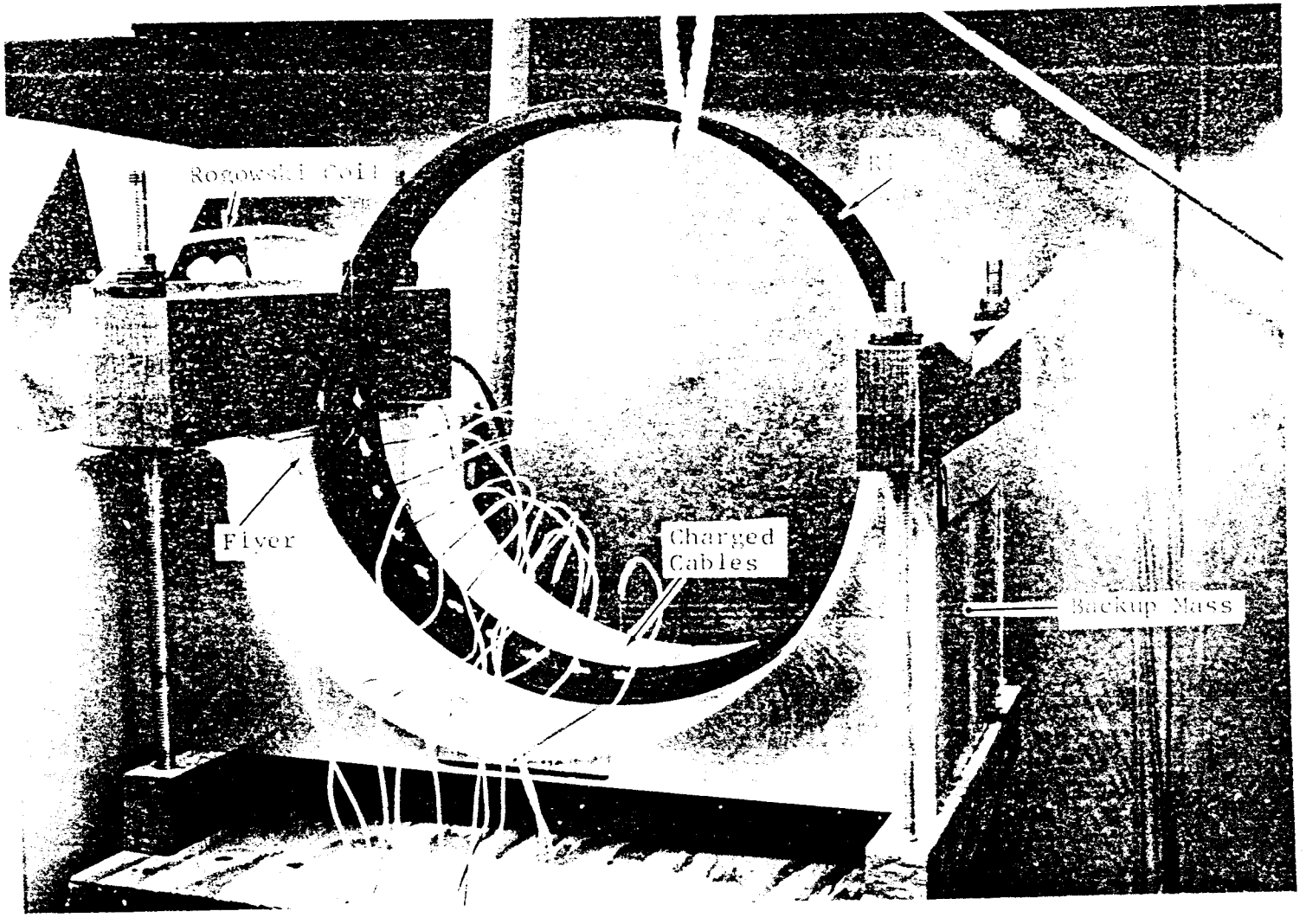

Figure 7. Cylindrical Ring-Flyer-Backup Mass Arrangement for Asimultaneity Assessment.

Since $V \propto \frac{1}{\zeta^2} \int_0^t i^2 \, dt$

and the maximum flyer velocity (at $\theta = 0°$) is

$$V_o \propto \frac{1}{\zeta_o^2} \int_0^t i^2 \, dt$$

and the desired flyer velocity distribution in θ is

$$V(\theta) \propto \frac{\cos \theta}{\zeta_o^2} \int_0^t i^2 \, dt,$$

then, $V(\theta) = V_o \cos \theta$.

This method can be shown to be valid for long, narrow flyers ($\delta_o << \lambda$). Magnetic field, B, maps between the flyer and backup mass show that an approximate cosine velocity can be produced by $\delta = \frac{\delta_o}{\sqrt{\cos \theta}}$ if $\frac{\delta_o}{\lambda} < .2$, where λ is the flyer length. Serious doubt is cast upon this method of shaping if $\frac{\delta_o}{\lambda} > .2$. To insure a "simultaneous" arrival of the flyer to the ring surface, the initial flyer-to-ring spacing must be $\sigma(\theta,o) = \sigma_o \cdot \cos \theta$. The maximum spacing, σ_o, must be chosen such that the flyer has reached terminal velocity before impact. Experimental evidence has indicated that if $\frac{\delta_o}{\lambda} > .2$ and $\delta = \frac{\delta_o}{\sqrt{\cos \theta}}$, the flyer will arrive at $\theta = \pm\pi/2$ first and sweep to $\theta = 0$. Figure 8 is a high speed framing camera sequence of a ring experiment (a = 2.5 in) where $\frac{\delta_o}{\lambda} = .32$ and $\delta = \frac{\delta_o}{\sqrt{\cos \theta}}$. In frame 3 the flyer has arrived at large θ and is sweeping toward $\theta = 0$. The time between frames is 4 microseconds. Figure 9 is the same experiment only with appropriate steps taken to produce a cosine velocity distribution. Frame 4 shows a very nearly simultaneous flyer arrival.

The case where the desired specific impulse is to be uniform for $-\pi/2 < \theta < \pi/2$ is obtained by letting $\tau = \tau_0$ and $z(\theta,0) = z_0$; thus the velocity of the flyer is $V = V_0$.

Simultaneity

As mentioned previously the simultaneity of the flyer-ring impact would be assessed. There are two obvious methods to gain information about time of arrival. One method has already been shown in Fig. 7. Very precise information about asimultaneity can be obtained from the pin-switch method at discrete locations on the ring periphery. Another method is to visually observe the flyer impact with a high speed framing camera. This was shown in Figs. 8 and 9. However, this method requires very high resolution and magnification for a quantitative assessment. An interesting derivative of the latter method is to use a transparent annular ring filled with argon gas, instead of the metal ring. As the flyer strikes the thin gas-filled annular ring, the radially directed compressive stress wave produced by the flyer causes the argon to emit visible light. Figure 10 is an axial view of the apparatus described above. The annulus is located at the periphery of the cylinder and is .010 inches thick. For this experiment the ratio $\frac{\tau_0}{\lambda} \approx .5$ so a sweeping load from $\theta = \pm 80^\circ$ to $\theta = 0$ is to be expected. Figure 11 is a sequence of high speed frames showing how the flyer does indeed sweep. The designed load was to be $I_0 \cos\theta$ and the initial flyer-to-cylinder spacing was made to produce a "simultaneous" impact.

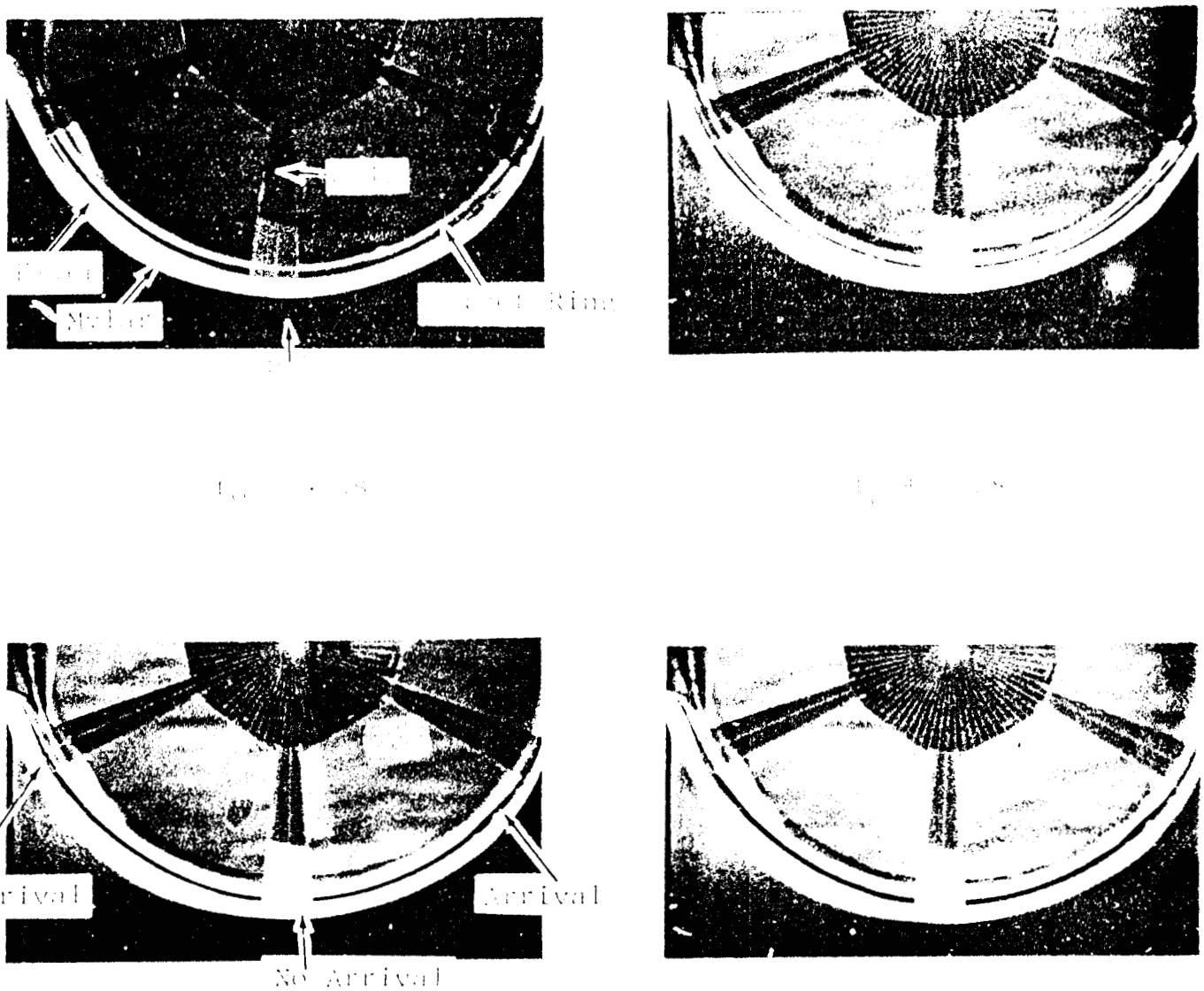

t_o + 12 μs

t_o + 16 μs

Figure 8. Example of Flyer Sweep.

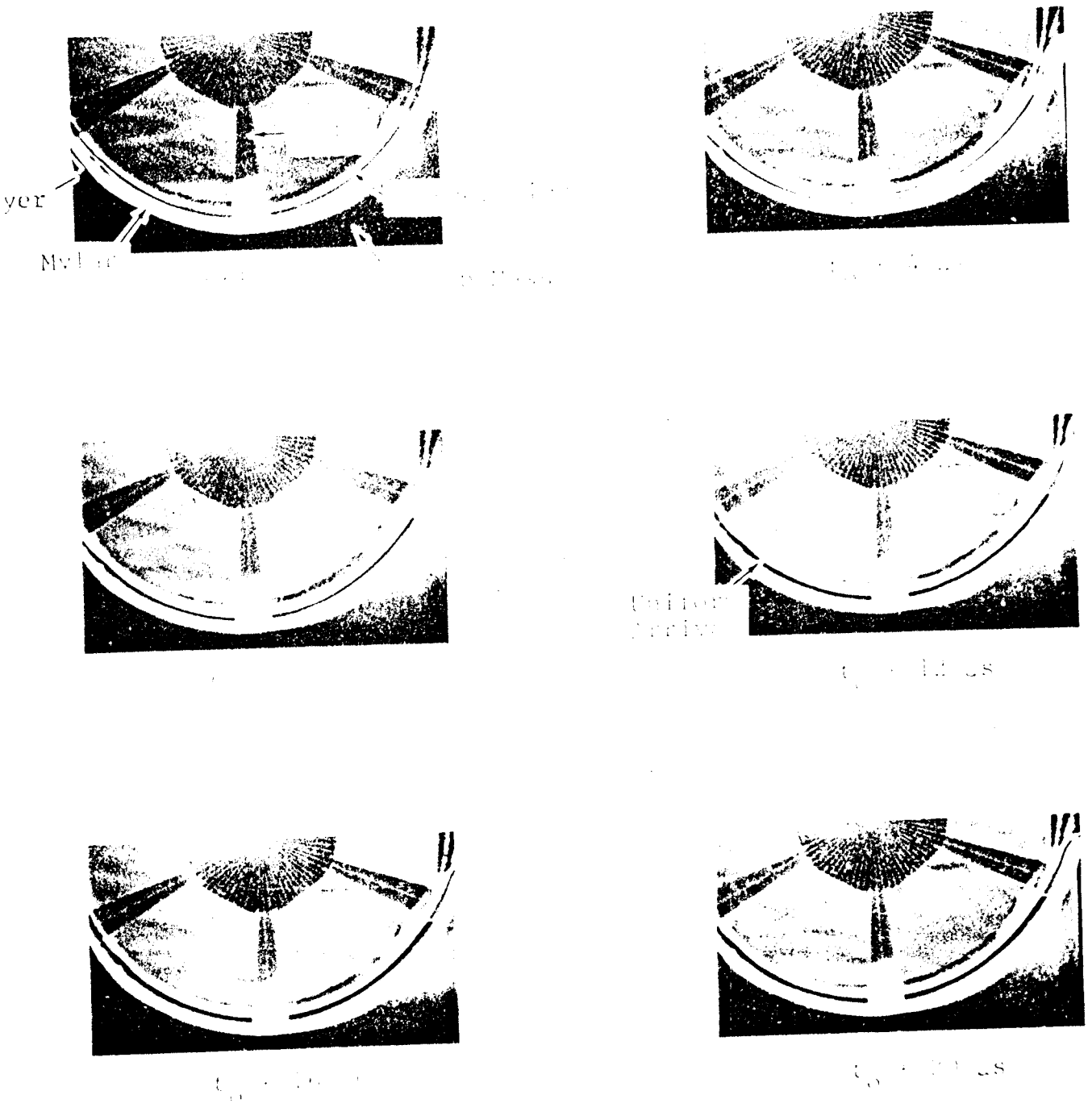

Figure 9. Corr ver Velocity Distribution to Produce More Simultaneous Arrival.

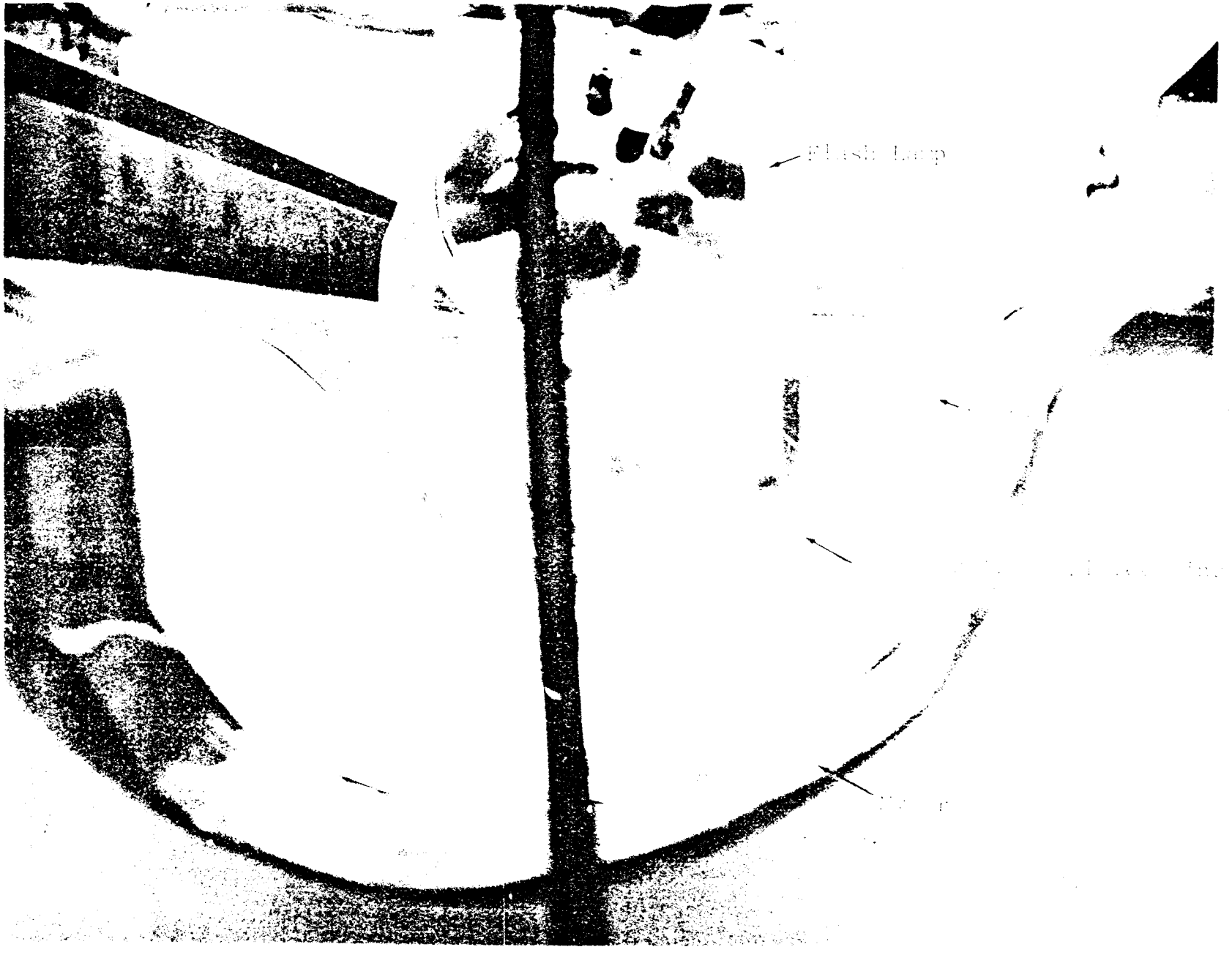

Figure 10. Still Photograph of an Optical Simultaneity Assessment.

Still

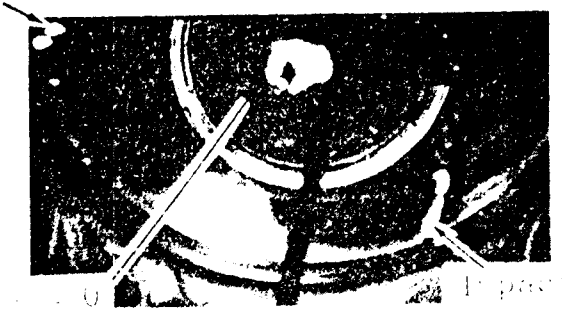

t_o + 4 μs

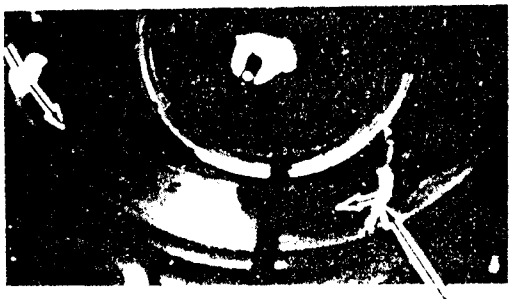

t_o + 8 μs

Light Flash Indicating Flyer Impact

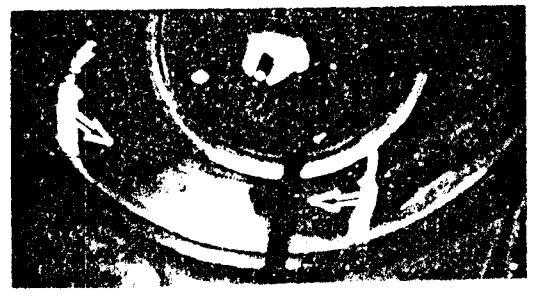

t_o + 12 μs

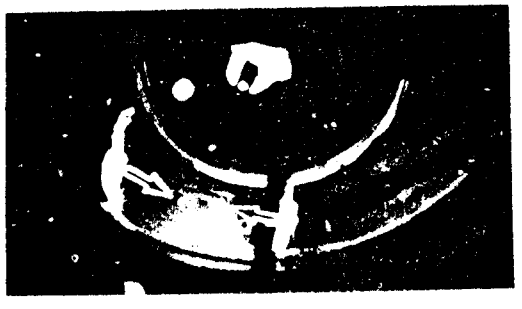

t_o + 16 μs

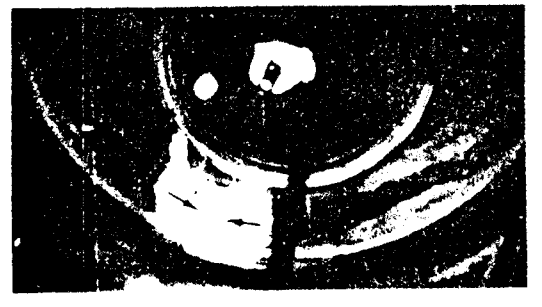

t_o + 20 μs

Figure 11. Frame Sequence of Flyer Sweep from Large θ Toward θ = 0.

The experimental results showed a sweeping flyer impact on the ring surface. Interestingly enough it was this experiment which prompted the investigation of the plate shaping methods explained previously.

One way to circumvent this problem is to direct the current in the axial sense instead of in the θ direction if $\frac{\delta_o}{\lambda} > .2$. For the experiments discussed in this paper $\frac{\delta_o}{\lambda} < .2$, so the current was directed in the θ direction. In the terminology used by flyer plate experimenters, these two methods of directing the capacitor bank discharge current are called solenoidal (for θ direction) and axial (for axial current direction).

For the structural experiments presented later in this paper the flyer velocity at $\theta = 0$ for both the level load and the cosine load was $\sim .105$ mm/μs. The asimultaneity, Δt, on the 12-inch diameter ring half surface was determined by the pin switch method to be .5 μs $< \Delta t <$ 1.1 μs for the level load case, where Δt was data accumulated over numerous calibration shots. For the cosine load case the range of asimultaneity for a number of calibration shots on 12-inch diameter dummy rings was 1.7 μs $< \Delta t <$ 2.6 μs. However, for the purposes of this paper the load will be "assumed" simultaneous. A later note will discuss the effects of this sweeping load on the ring response.

Flyer Buckling

A problem which must be avoided in flyer plate loading of cylindrical geometries is that of flyer buckling. As the

rapidly moving larger radius flyer converges on the smaller radius cylinder through large displacements, it wrinkles severely because the flyer is fixed at both ends. This effect is demonstrated in Fig. 12, which is a high-speed framing camera sequence looking at the flyer edge. Each narrow, horizontal black line represents .100 inches of vertical displacement. The radius of the flyer is 2.5 inches, and the flyer thickness is 0.012 inches. The residual image on each frame is the flyer after it has traveled nearly 1. inch. The later frames show that the flyer has begun to wrinkle after 0.150 inches of displacement. The highest order buckling occurs at $\theta = 0°$ which restricts the maximum flight distance before buckling. The buckling problem can be avoided by maintaining small flight distances (< 0.100 inch) and increasing the flyer thickness.

Another problem associated with the buckling tendency is edge curl-up. The magnetic field lines near the flyer edges are no longer parallel to the flyer and backup mass as they are near the center of the flyer. This creates forces tending to curl the flyer as it moves away from the backup mass. Figure 13 is a framing sequence looking down on a 3.0-inch radius, 2.5-inch wide flyer as it moves toward the observer; the frames are 3 μs apart. The grid lines on the flyer face serve to accentuate any wrinkling. Edge curl-up is noticeable after the second frame and becomes more pronounced in succeeding frames. Buckling as described in the previous paragraph can be seen by frame 5. Since the edge curl-up occurs before the flyer impacts the ring, the flyer edges must not strike the

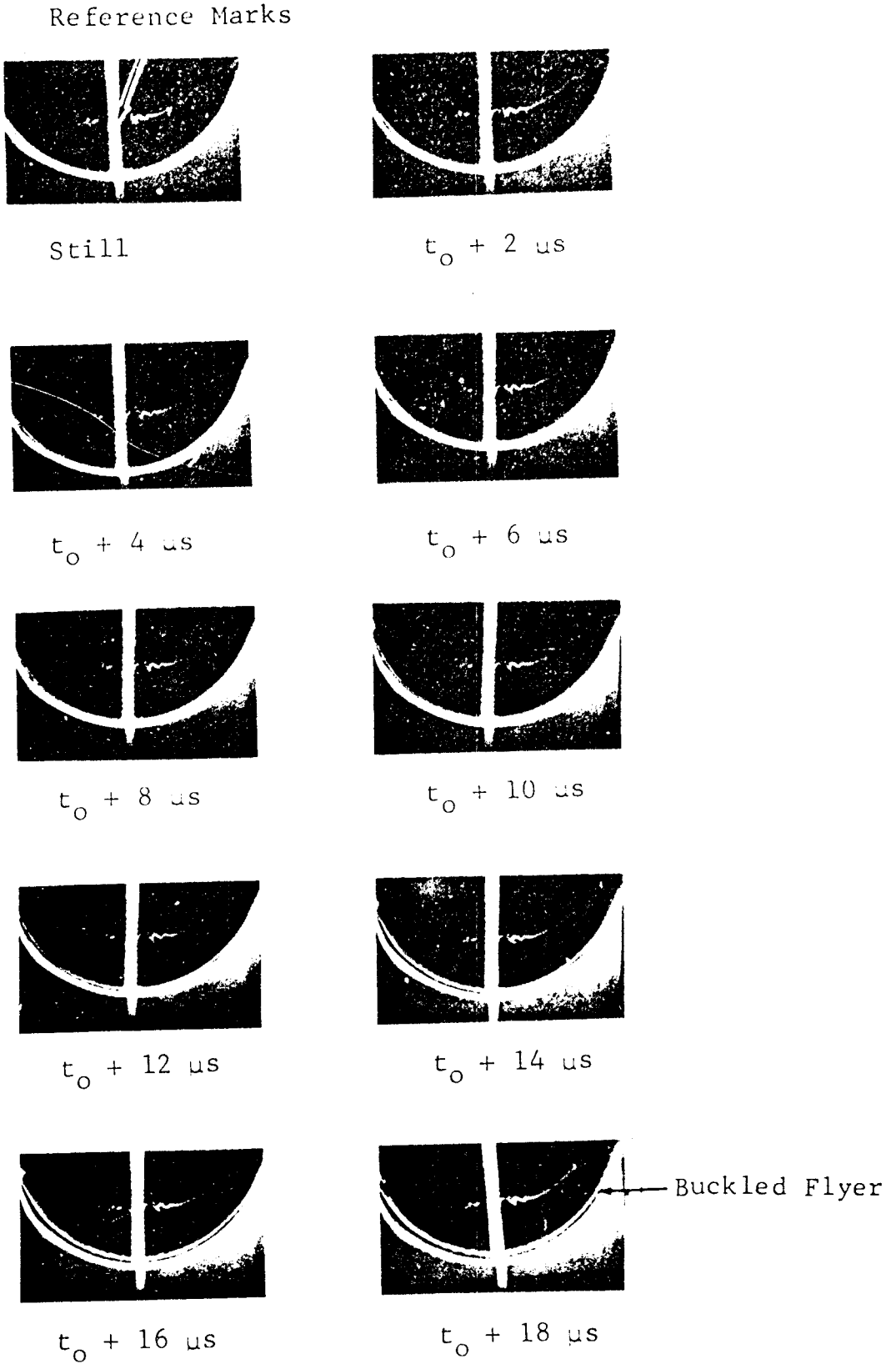

Figure 12. Frame Sequence of Flyer Buckling--Edge View.

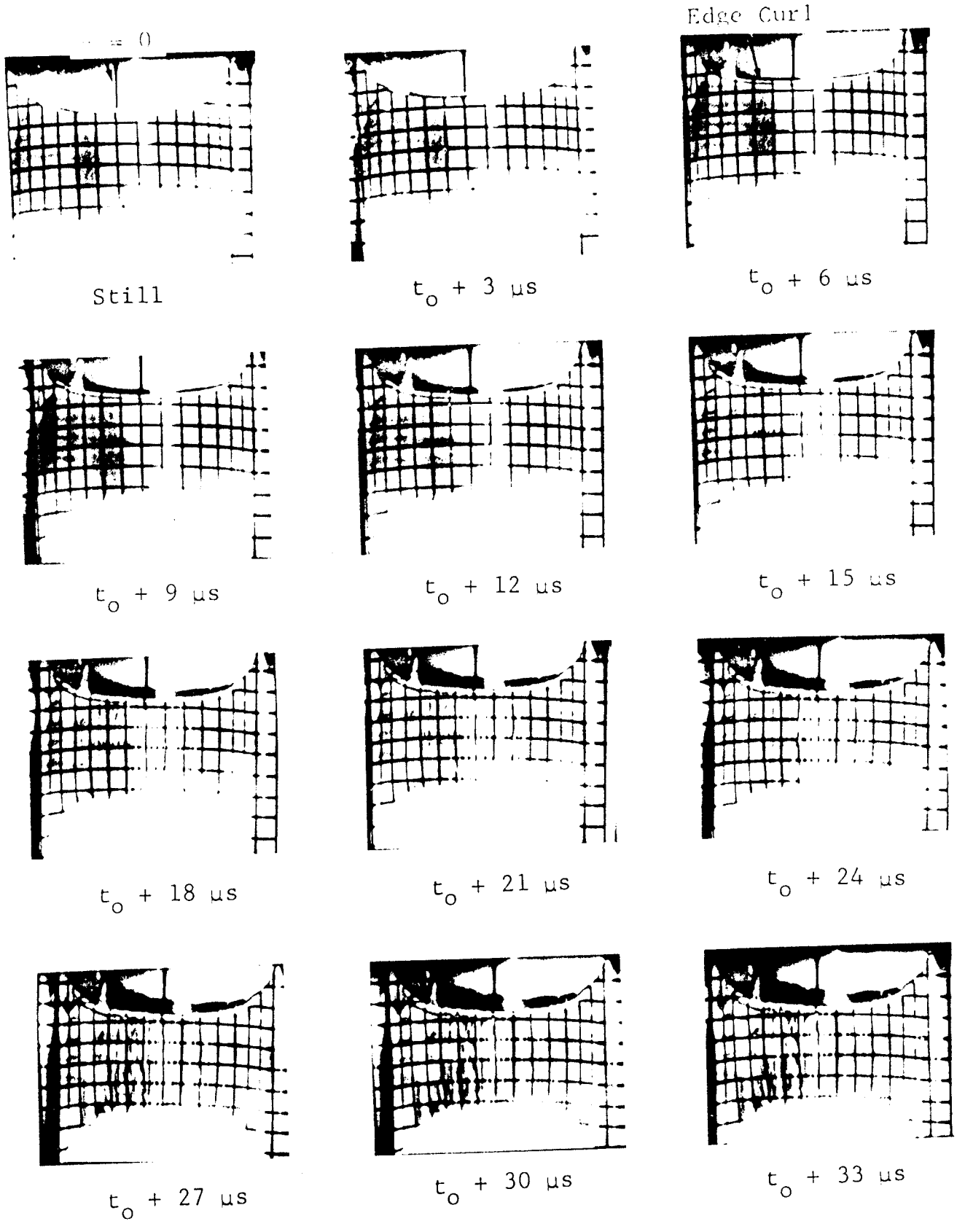

Figure 13. Top View of Flyer Showing Edge Curl and Buckling.

ring surface. The flyer is made wider than the ring, and guard rings are used on each side of the ring to prevent edge impact and to prevent the flyer from wrapping itself about the slower moving ring.

Ring Model

The ring selected for study was 4340 steel, a = 5.875 inches and h = .250 inches. Steel 4340 was chosen because of its high yield point and high spallation pressure threshold. Since the response was to be elastic at the level of impulse chosen, no permanent deformation or spallation was wanted.

Strain Measurement Methods

The stated purpose of the experiment was to measure the response of the ring model. Strains in the ring were measured with Kulite M(12)DGP350-500 semiconductor strain gages. Further information about semiconductor gage operation can be found in Ref. 9. The gages were located at $\theta = 0_-, \pi/2_-, \pi_+, \pi_-$, and $3\pi/2_-$, where the signed subscripts (-) and (+) denote inner and outer surface locations respectively. The Kulite DGP350 is a dual element gage with one element having a positive gage factor, $F_1 = \frac{\Delta R/R_1}{\varepsilon}$, ($F_1 \approx 135$) and the other a negative gage factor, $F_2 = -\frac{\Delta R/R_2}{\varepsilon}$, ($F_2 \approx -115$), where R is gage resistance and ε is the local strain. This gage has the advantages of high gage factor, temperature compensation, and a constant gage factor over the range of strain in this experiment. Figure 14

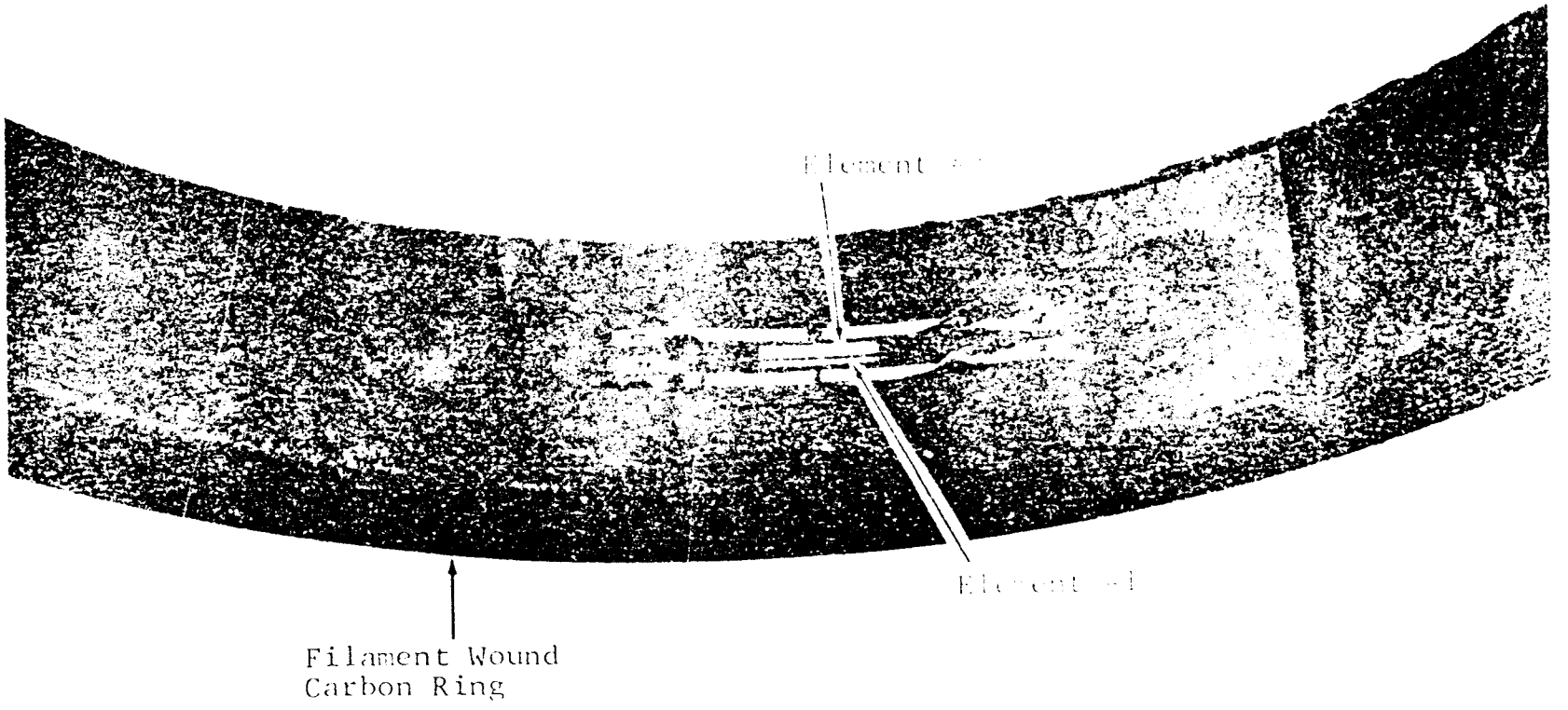

Figure 14. Semiconductor Strain Gage Arrangement.

shows a typical gage installation, in this case on a carbon filament, composite ring. Each gage formed the two active arms of a Wheatstone bridge biased with 12 volts. The signal from the bridge circuit was recorded directly on a Tektronix 556 oscilloscope, using Tektronix 1A2 signal amplifiers, and photographed. Output voltages greater than .5 volt were not uncommon. Because of the high magnetic field, B, produced by the capacitor discharge which induced unwanted common mode signals in the circuit, the common mode rejection capability of the 1A2 amplifier in the differential mode was necessary.

The current, i(t), in the system was measured with a Rogowski loop. The signal from the loop was integrated and recorded on an oscilloscope.

The flyer plate displacement S(t), was determined with a high speed streak camera. The flyer current and displacement were presented in the previous section. The strain data are presented in the next section.

Experimental-Theoretical Ring Response

The elastic response of circular rings to side pressure pulses has been presented by numerous authors.[10,11] The solutions given in Refs. 10 and 11 excluded the effects of bending. Humphrey and Winter, Ref. 12, showed that bending effects were negligible for the very early time response of thin rings. It was shown in Ref. 12 that after the first stress cycle the purely membrane response was not a good model of the actual ring

response. Figures 15 and 16 are the measured oscilloscope traces from the semiconductor strain gages for the case where $P(\theta) = P_o$ and $P(\theta) = P_o \cos\theta$ respectively. Figure 15b is a time expansion of Figure 15. The pressure pulse duration delivered to the structure was < 200 nanoseconds, so by the criterion set forth in Ref. 12 the surface loading is considered impulsive. Figure 17 is the measured response at $\theta = \pi/2$, for $P(\theta) = P_o$, compared with the predicted response due to Humphrey and Winter. Figure 18 is the measured response at $\theta = \pi$, for $P(\theta) = P_o$, compared with the predictions of Humphrey and Winter. The comparison at $\theta = \pi/2$ is not so good as it is at $\theta = \pi$ because of the local flyer perturbation at $\theta = 80°$. The fact that the load does not extend over a full $\theta = 180°$ must be taken into consideration when comparing theory and experiment at $\theta = \pi/2$. The actual contribution of the flyer plate ends to the ring response is presently being studied.

The second experiment was identical to the first except the pressure distribution to the ring was $P(\theta) = P_o \cos\theta$ ($-85° \leq \theta \leq +85°$). Figure 19 is the measured response at $\theta = \pi/2$ compared with the predicted response for $P(\theta) = P_o \cos\theta$. Figure 20 is the measured response at $\theta = \pi$ compared with the theoretical elastic response for a cosine, impulsive pressure distribution. The same arguments as used before should be applied to the poorer comparison at $\theta = \pi/2$.

It should be noted that comparison between theory and experiment for both pressure distributions (level and cosine) becomes poorer as time increases. This could indicate that

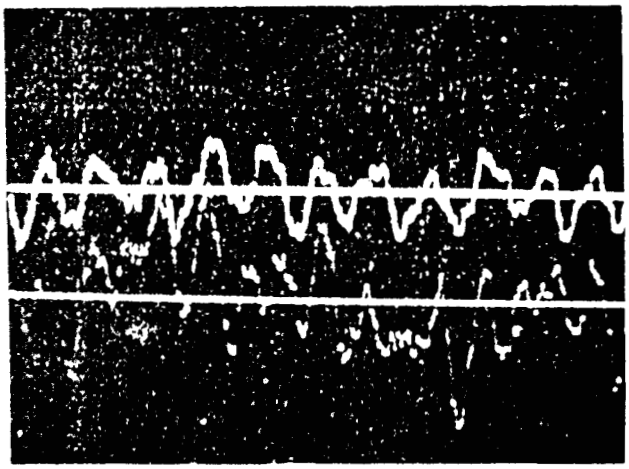

Fig. 15a. Strain vs. Time at $\theta = \pi/2$ and $\theta = \pi$ for $P(\theta) = P_o$

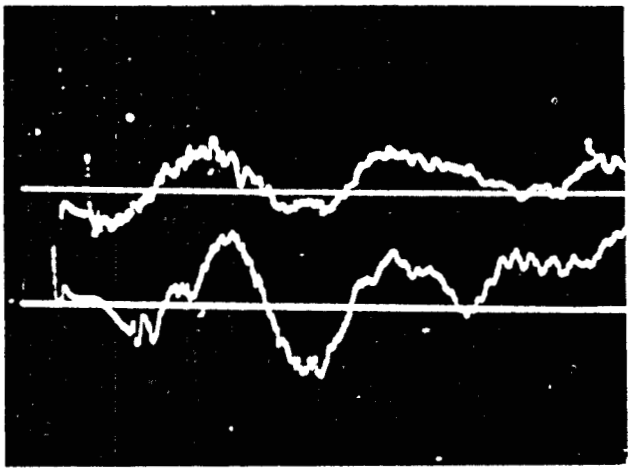

Fig. 15b. Same as 15a except a time expansion of early response

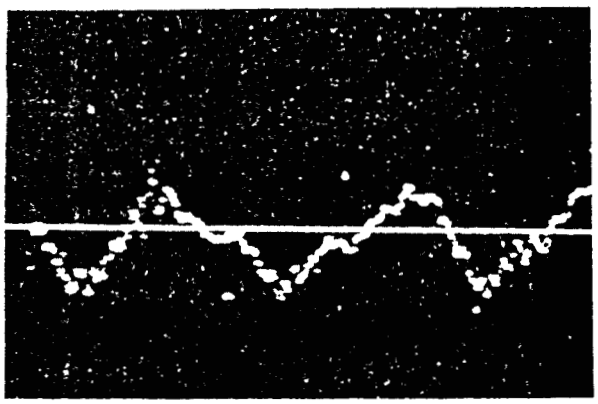

Fig. 16a. Strain vs. Time at $\theta = \pi/2$ for $P(\theta) = P_o \cos\theta$

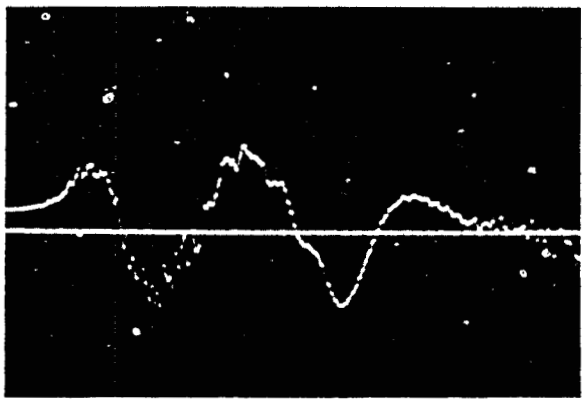

Fig. 16b. Strain vs. Time at $\theta = \pi$ for $P(\theta) = P_o \cos\theta$

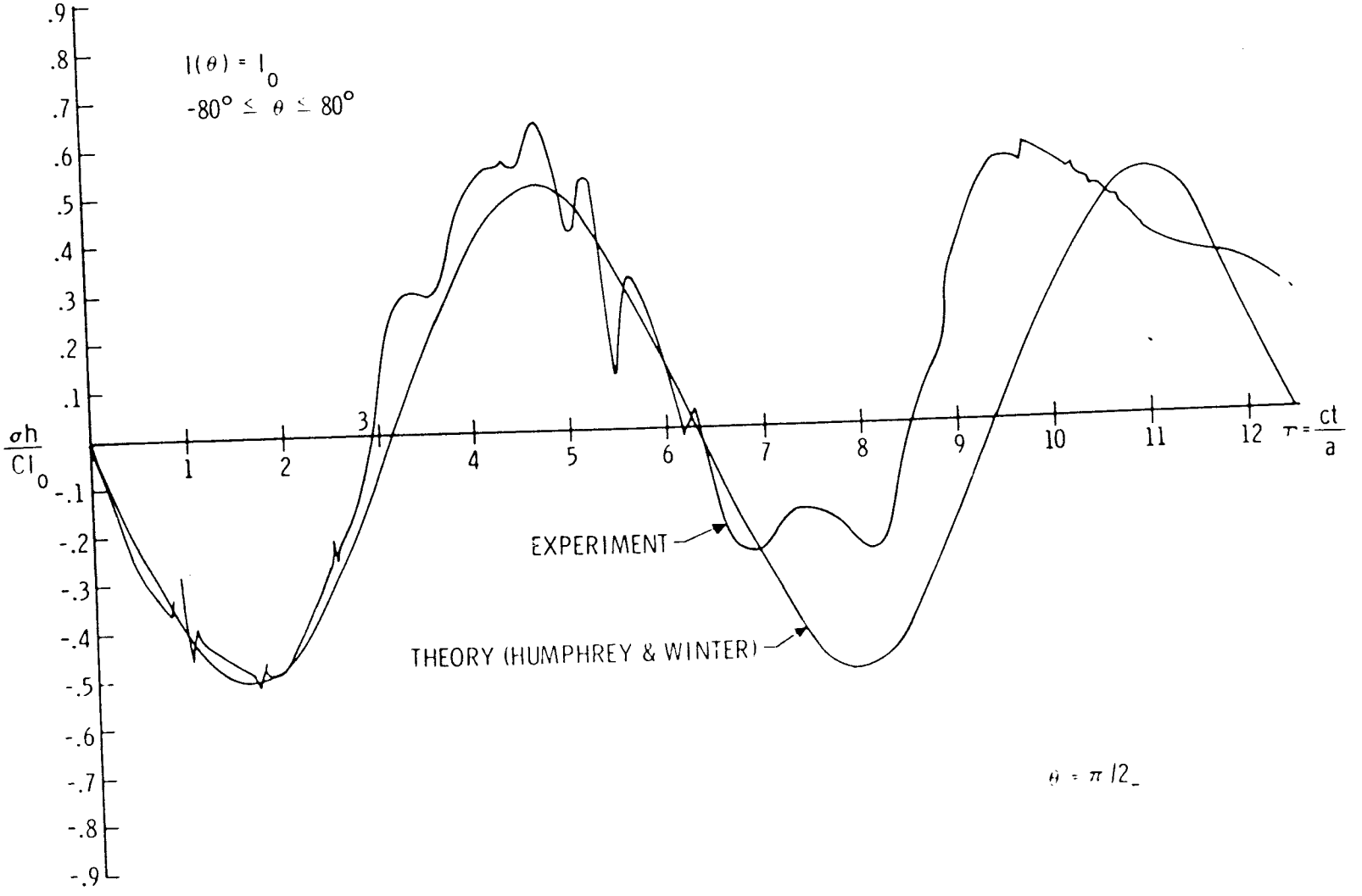

Figure 17. Nondimensional Stress vs. Time at $\theta = \pi/2$ for Level Load--Theory vs. Experiment.

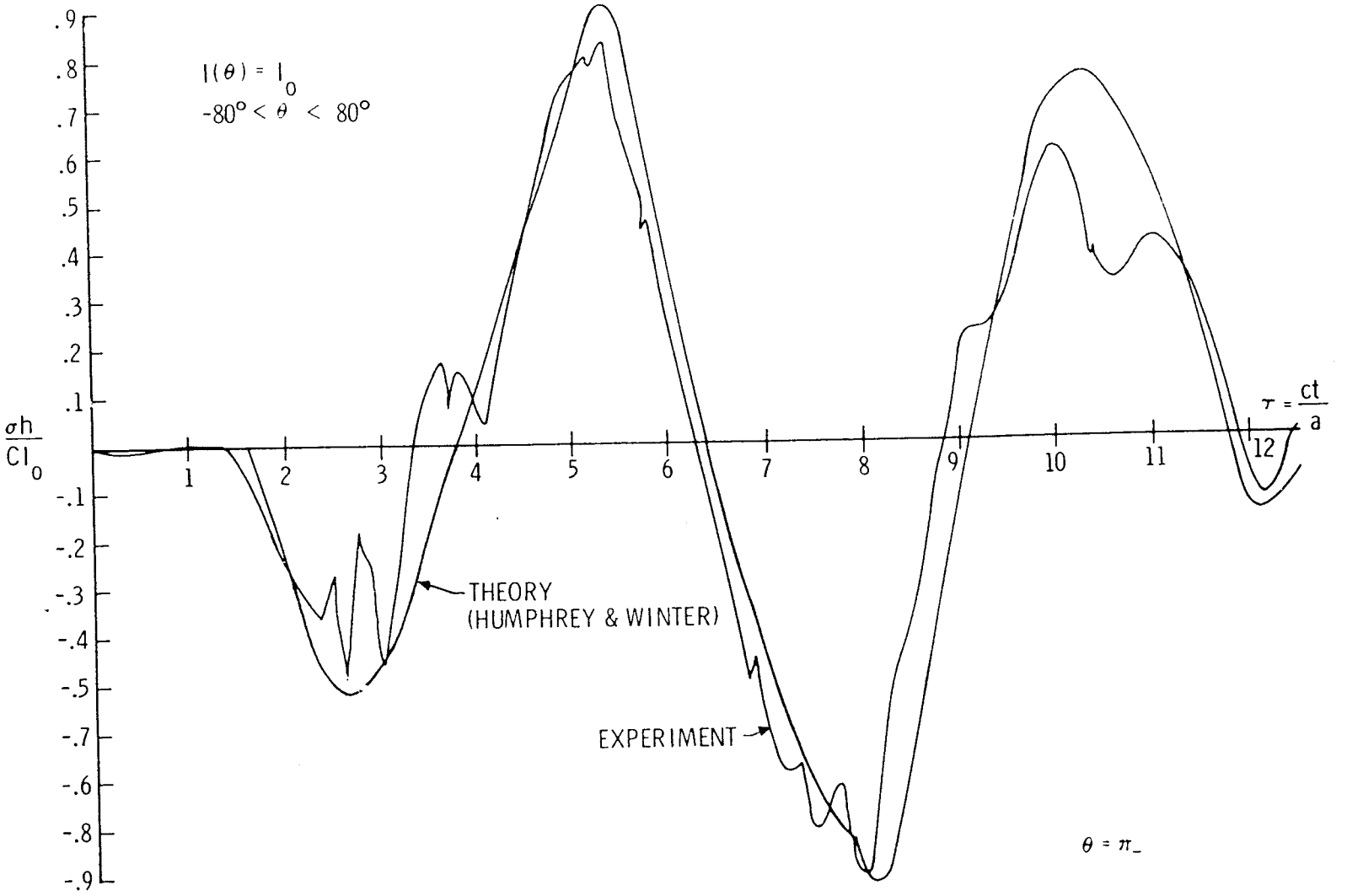

Figure 18. Nondimensional Stress vs. Time at $\theta = \pi$ for Level Load--
Theory vs. Experiment.

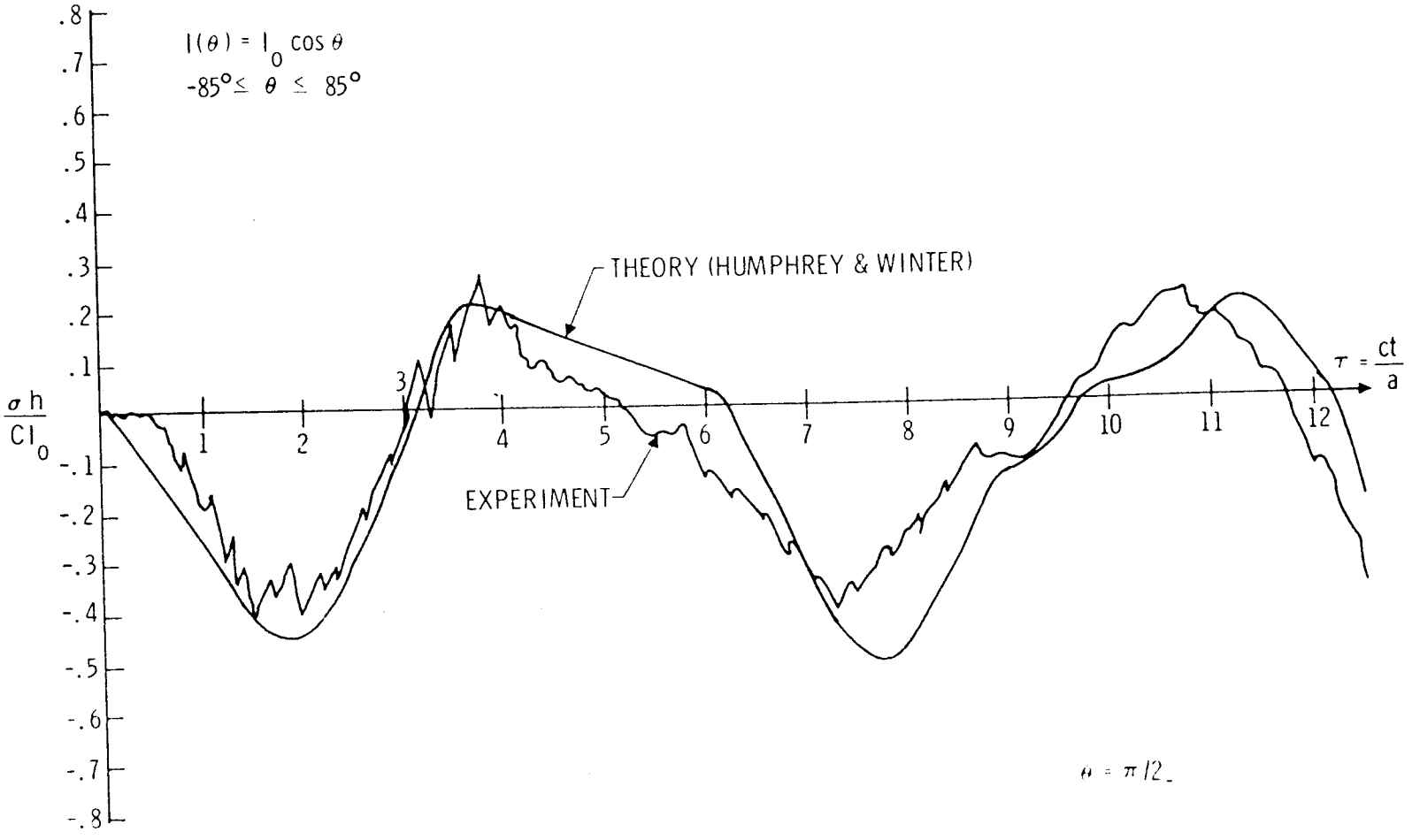

Figure 19. Nondimensional Stress vs. Time at $\theta = \pi/2$ for Cosine Load--Theory vs. Experiment.

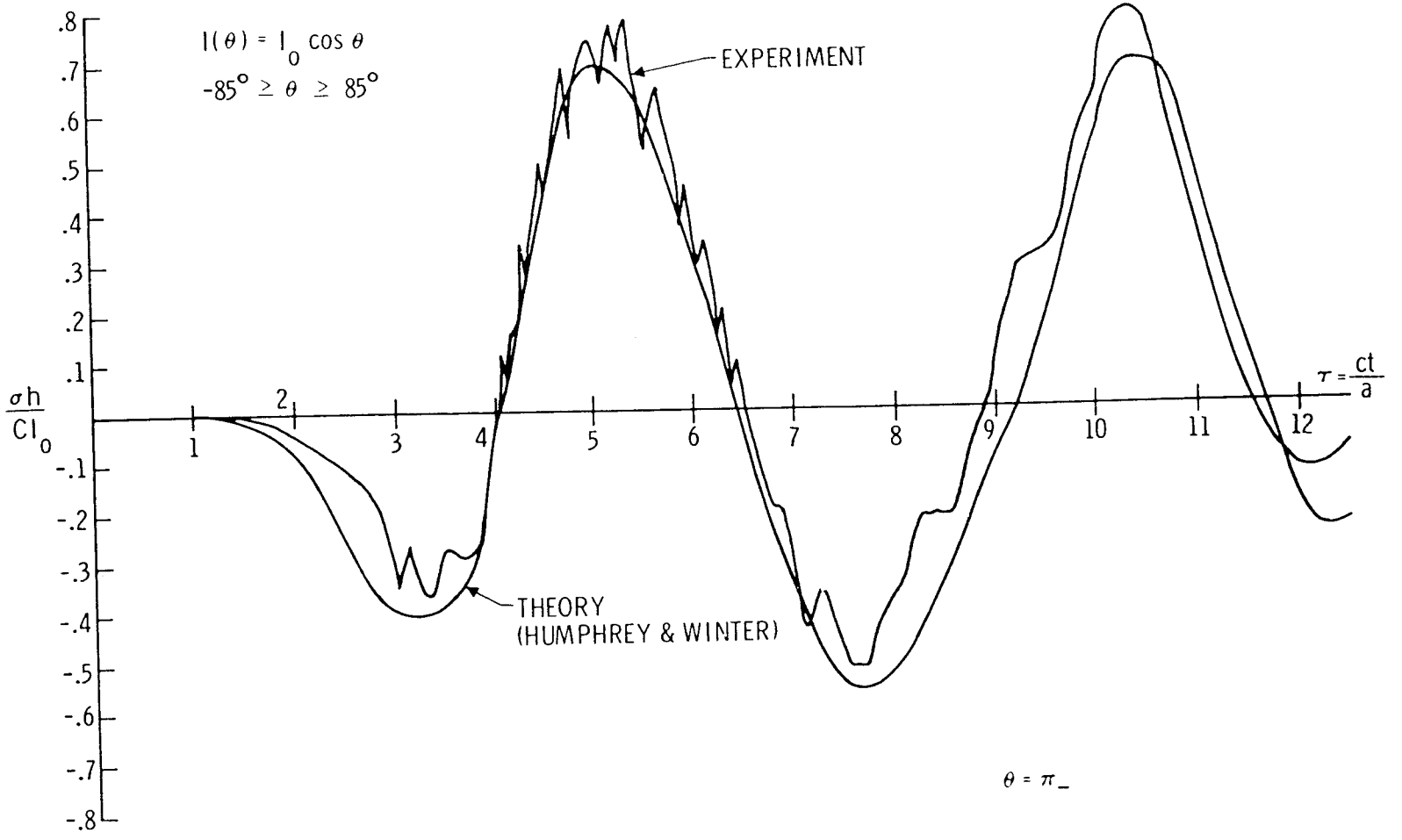

Figure 20. Nondimensional Stress vs. Time at $\theta = \pi$ for Cosine Load--
Theory vs. Experiment.

the model set forth in Humphrey and Winter is sufficient for very early ring response but inadequate for late time response. On the other hand, the inability to load exactly 180° could create discrepancies which become amplified in time. Thus it is unfair to compare a theory which loads a full half circumference to an experiment that loads only 170° of ring surface. Through cooperation with Applied Mechanics Division 1544 this problem is being resolved.

Conclusions

An attempt was made in this paper to present the magnetically-propelled flyer plate technique as used to impulsively load thin rings. It was shown that the lumped parameter, time varying, series L-R-C circuit is a reasonable approximation of the capacitor discharge system. Fair agreement was obtained between the theory outlined in the first section and the experimental results for the flyer motion.

Structural response experiments were conducted on rings ($a/h = 23.5$) using the magnetically-accelerated flyer plate technique. Reasonably good agreement between the predicted ring response and the measured response was obtained at early times for two specific impulse distributions.

It has been shown that the experimental method could be fairly well defined, and the membrane and bending theory for the early time ring response was adequate. It then seems likely that the flyer plate method will be used to load more complex

structures such as composite shells. The advantages of very short pulse durations and "simultaneous" loading of large areas will in time replace the conventional axial sweeping explosive method for obtaining the response of large and small structures.

Acknowledgments

The author wishes to acknowledge the help of C. SifreSoto who performed all the experiments. The high speed photographic coverage of T. A. Leighley is also acknowledged.

References

1. Wenzel, A. B. and Baker, W. E., "The Use of Light-Initiated Explosives for the Impulsive Loading of Structures," Institute of Environmental Sciences, 1970 Proceedings.

2. Stanton, P. L., "Explosive-Driven Flyer Plate Plane-Wave Generator," Engineering Mechanics Research Lab. Contract Report 58-1692 for Sandia Laboratories SC-CR-68-3672.

3. O'Rourke, R. C., Dobbie, C. B., Protopapa, S., Smollen, L. E., Phillips, C. O., and Farber, J. Z., "Progress Report--Impulsive Load Tests on Cylindrical Assemblies, Phase I and II," EG&G Technical Report B-3147, EGG-1183-235, September 1965.

4. Nelson, D. B., "Resistance Effects on the Performance of Magnetically Driven Flyer Plates," Sandia Laboratories Report, SCL-DR-69-34, May 1969.

5. Reynolds, R. W. and Jacobson, R. S., "Numerical Predictions of the Motion of Magnetically Accelerated Flyer Plates," Sandia Laboratories Report, SCL-DR-69-44, July 1969.

6. Tucker, W. K., "Two Computer Programs for Flyer Plate-Capacitor Bank Analysis," Sandia Laboratories Report, SC-DR-70-122, February 1970.

7. Cnare, E. C. and Freeman, J. R., Private Communication.

8. Farber, J. Z., "Diffusion of Damped Sine Wave Magnetic Fields into Metals," EG&G Technical Report B-3307, EGG-1183-299, May 1966

9. Dorsey, J., "Semiconductor Strain Gage Handbook," BLH Electronics Technical Report, Sections I-VII, October 1964.

10. Payton, R. G., "Dynamic Membrane Stresses in a Circular Elastic Shell," Journal of Applied Mechanics, 28, 1961, pp. 417-420.

11. Forrestal, M. J., Alzheimer, W. E., and Schmitt, H. W., "Thermally Induced Membrane Stress in a Circular Elastic Shell," AIAA Journal, 6, May 1968, pp. 946-948.

12. Humphreys, J. S. and Winter, R., "Dynamic Response of a Cylinder to a Side Pressure Pulse," AIAA Journal, 3, January 1965, pp. 27-32.

Distribution:

M. J. Forrestal, 1223
M. J. Sagartz, 1223
W. E. Alzheimer, 1517
R. T. Othmer, 1544
R. L. Parrish, 1544
W. A. Sebrell, 1544
L. T. Wilson, 1544
R. A. Benham, 7342
R. I. Butler, 7342
J. L. Cawlfield, 7342
F. H. Mathews, 7342
C. SifreSoto, 7342
H. C. Walling, 7342 (11)
W. K. Tucker, 7345
W. F. Carstens, 3410, Attn: R. S. Gillespie, 3411
B. F. Hefley, 3421
C. H. Sproul, 3428-2 (12)
Livermore Library, 8232